

MIRAGE Emitter Improvements & Technology Review

Steve Solomon

Acumen Consulting, PO Box 6084, Santa Barbara, CA 93160

Alan Irwin, Jim Oleson, Kevin Sparkman

Santa Barbara Infrared, Inc., 312 N. Nopal Street, Santa Barbara, CA 93103

Anthony Gallagher, William Lin, Jianmei Pan,

Rockwell Science Center, 1049 Camino dos Rios, Thousand Oaks, CA 91360

ABSTRACT

Data is presented that resulted from a major science & engineering study aimed at improving the maximum operating temperature of the Mirage emitter array. The past year has seen substantial improvements in the Mirage emitter pixel, resulting in high operability and yield, and most recently, a highly stable MWIR apparent temperature of 700K. Advanced diagnostic techniques were used in order to identify and optimize the emitter fabrication process. First principles were employed, where appropriate, in order to gain insight into the physical mechanisms responsible for driving each of the emitter figures of merit. A materials study was performed in order to select the best material stack, and a variety of anneal conditions were used to determine which produced the highest and most stable temperatures. Optical constants of the materials were measured over the IR band of interest in order to allow more accurate modeling of the emissivity.

Keywords: Infrared, Scene Simulation, Scene Projection, and Emitter Array

1 INTRODUCTION

SBIR has attained highly stable emitters with MWIR apparent temperatures of 700K. This success has been the result of a major, cross-disciplinary technology improvement effort. Physical modeling and materials characterization were the primary thrusts in the development effort that resulted in improved device performance.

2 MIRAGE EMITTER

Figure 1 shows a microphotograph of a portion of the Mirage emitter array. The emitters are fabricated by Rockwell Science Center (RSC) using the Transfer Thin Film Membrane (TTFM) process. The TTFM process allows initial emitter material processing to be performed independently from any RIIC processing. After emitter material and RIIC die have been partially processed, they are joined together in a step called mating. The TTFM process offers the advantages of wafer level emitter material annealing (prior to mating with the RIIC), and parallel processing of emitter material and RIIC die. In addition, reduced RIIC loss is realized by ensuring that only good emitter material is mated to known good RIIC die¹.

The first proof-of-concept emitter was fabricated in the Spring of 1999 at RSC. SBIR and RSC have come a long way up the learning curve since that first emitter. There has been considerable modification and improvement in both the processing and the devices over the intervening period, which has accelerated over the past year. As an example, we have employed advanced diagnostic tools such as focused ion beam (FIB) to cross section finished devices in order to resolve process issues, resulting in high yields and operabilities consistently greater than 99.5%².

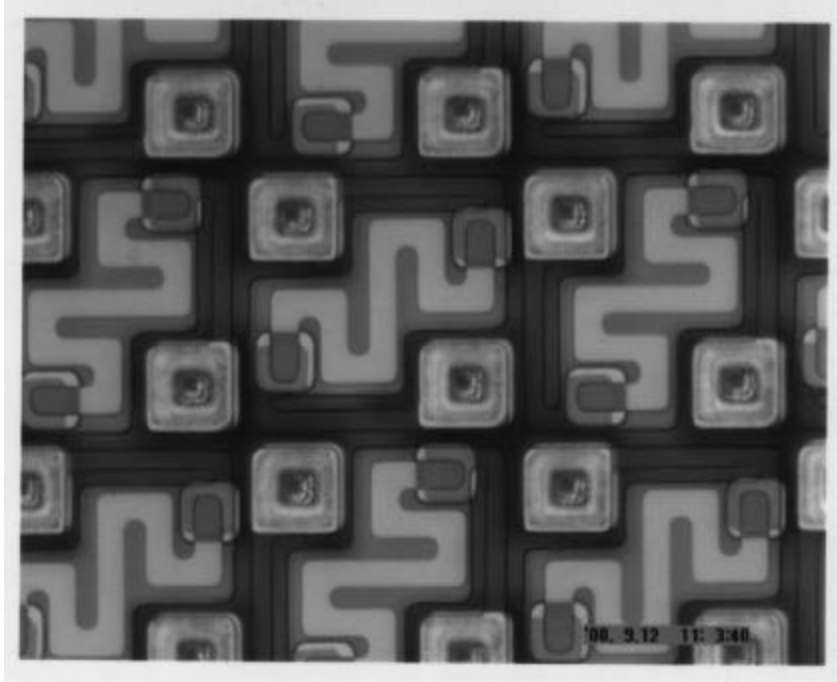


Figure 1 – Microscope photograph of a subsection from a Mirage emitter array.

3 TECHNOLOGY DEVELOPMENT

We have advanced emitter technology at SBIR & RSC via a balanced approach to operational improvement of the emitter array. The baseline process and the resulting devices were fully characterized in order to provide a roadmap for performance improvements. Where appropriate, physics-based models were developed and verified using device data. Once validated, these models played a major role in determining how to obtain the desired performance improvements. In addition to the models, considerable effort was expended in the area of materials research and experiment. When taken together, the end result was a robust anneal process, resulting in exceptionally stable emitters that easily reached MWIR apparent temperatures of 700K.

3.1 Device physics & modeling

The temporal behavior of a pixel is determined by the balance between the power input to the pixel and the power loss mechanisms. The power input is simply that of Joule heating, and the loss terms are given by thermal conductance through the legs and radiative losses. This is expressed by the first order, non-linear differential equation:

$$m \cdot c_p(T) \frac{dT}{dt} = i^2 R(T) - \frac{A_{leg}}{l_{leg}} \lambda(T) (T - T_{sub}) - 2A \epsilon \sigma T^4 \quad (1)$$

where m is the mass of the emitter pixel, c_p is the heat capacity, T is the pixel temperature, i is the pixel current, R is the pixel resistance, A_{leg} and l_{leg} are the cross sectional area and length of the legs, respectively, λ is the thermal conductivity of the leg, T_{sub} is the substrate temperature, A is the pixel area, ϵ is the average broadband emissivity of the pixel, and σ is the Stefan-Boltzmann constant. This equation was used to model the temporal behavior of the pixel (*i.e.* to validate the measured radiance rise and fall times, see 4.4 Temporal response). Note that this equation describes the physical temperature of the emitter pixel, rather than the apparent temperature or radiance. The primary assumption implicit in this equation is that the thermal conductance and heat capacity are separable (*i.e.* that the conductance path is largely through the leg and that the heat capacity is mostly in the pixel body itself), which is the case for the Mirage geometry.

This equation also illustrates the various parameters that the emitter designer has available to adjust the performance figures of merit: pixel geometry and material, leg geometry and material, heater element resistance and drive voltage (or current). The only remaining measure of importance for emitters is the in-band emissivity, which is not contained in this equation, thus leaving the designer with an additional degree of freedom in the emitter cavity stack.

Under steady state conditions, the pixel has reached its final, constant temperature, so that equation (1) reduces to:

$$i^2 R(T) = \frac{A_{leg}}{l_{leg}} \lambda(T) (T - T_{sub}) + 2A\epsilon\sigma T^4 \quad (2)$$

This equation was used to calculate the physical temperature attained by the emitter pixel, which was then used to determine the emissivity (see 4.3 Emissivity).

The material parameters used in equations (1) and (2) are functions of temperature. It is enormously difficult to obtain measurements of the heat capacity and thermal conductance of thin films over the broad operating temperature range of the emitters, so the functional behavior of these two parameters was taken from the literature in the models presented here. We intend to measure these parameters in the near future in order to better understand the behavior of the materials used in the emitter stack, and hence, be able to optimize device performance.

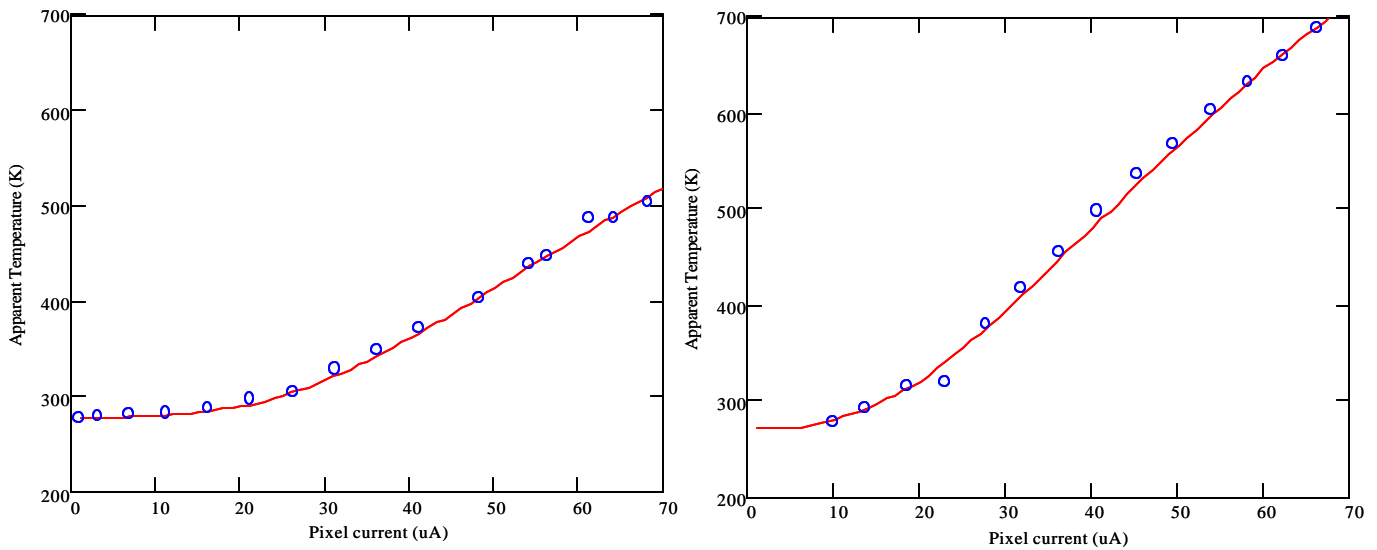


Figure 2– Apparent MWIR temperature for the baseline emitter (left, M13) and the new, high temperature emitter (right, M14). The open circles are the measured data and the solid lines are the model predictions from equation (2)

3.2 Materials Characterization

A materials study was undertaken in which a variety of different materials were characterized for possible inclusion into the emitter cavity stack. The characterization consisted of measuring the optical and electrical properties of each material as deposited and after a variety of different anneals were performed. The results of this experiment enabled us to select the optimal materials and anneal conditions required for stable, high temperature operation.

3.2.1 Optical Constants & Anneal

We determined that it was important to directly measure the optical constants (index of refraction and the absorption coefficient, n and k , respectively) of the emitter stack components for two reasons: 1) the method of measuring DC electrical

resistance and inferring the optical constants results in poor emissivity predictions at shorter wavelengths because the approximations used to infer n and k from the conductivity break down in the region around $8\text{--}10\mu\text{m}$ and below, and 2) the conductivity model cannot account for anomalous dispersion (absorption features), which are known to be present in a variety of dielectrics and metallic oxides. Additionally, we are in the process of connecting the two methods using the Drude theory and expect to publish the results in the near future. These measurements aid in both constructing as well as validating the device models, thereby providing guidelines for design improvements.

The optical constants were measured via multispectral (and multi-angle) ellipsometry over the spectral band from $400\text{nm}\text{--}15\mu\text{m}$. These measurements were performed on each of the films in the as-deposited state and after a variety of different anneals were performed. X-ray photoelectron spectroscopy was also performed in order to determine the nature of the chemical changes across films and film interfaces that resulted from the various anneal conditions. These latter data serve to provide a physical/chemical understanding of the observed changes that occur in the apparent temperature with anneal, and enable the development of improved, more stable materials and anneal conditions. Figure 3 shows the results of these experiments for a particular material under consideration for inclusion in the stackup. From this figure, it is clear that the optical properties of this film (and hence the emissivity of the stack) are strong functions of the anneal conditions.

Performing the measurements at optical wavelengths and correlating these with the IR measurements has enabled the development of in-process tests (most foundries have single optical wavelength ellipsometers). This is an important throughput and yield (cost) issue; the earlier in the process inadequate film properties can be identified, the fewer resources are wasted in processing poor devices.

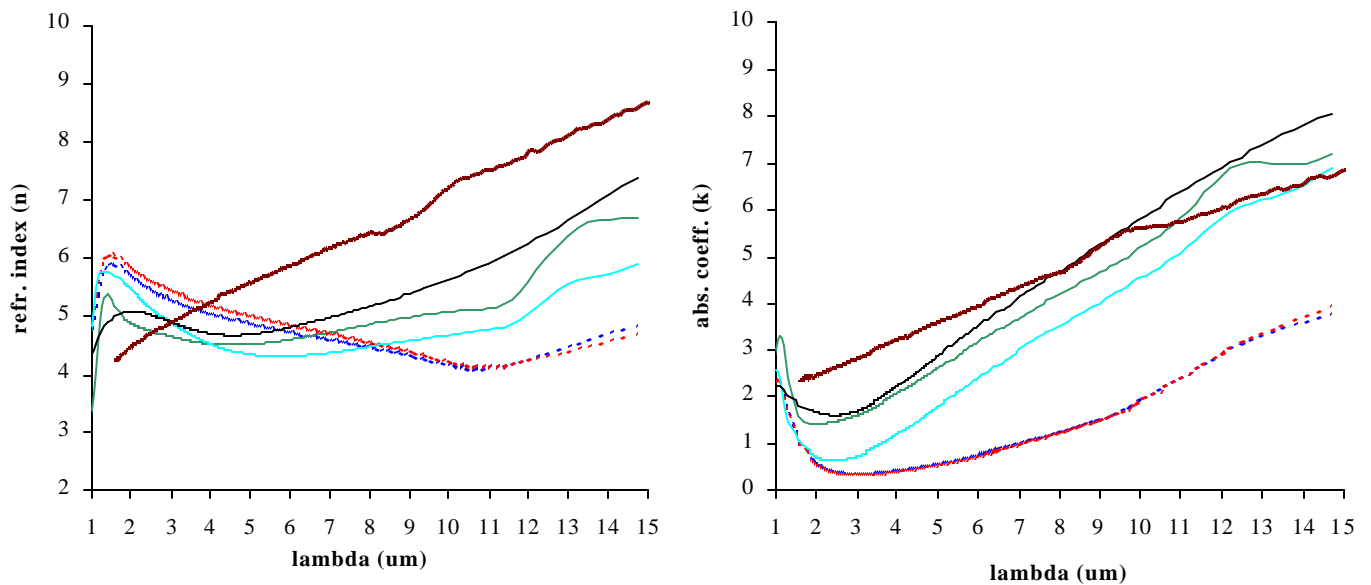


Figure 3- Optical constants (n & k) measured via multispectral ellipsometry for a potential material. The bold curve shows the film properties as-deposited, while the remaining curves show the change in optical properties that resulted from various anneal conditions.

3.2.2 Heater Resistance vs. Temperature

The resistance as a function of drive voltage was measured in order to observe the change in heater resistance with operating temperature. As expected, we observed the resistance to fall monotonically with drive voltage. In order to determine the resistance as a function of temperature ($R(T)$), the following algorithm was used:

- 1) equation (2) was used to calculate the physical temperature as a function of drive voltage,
- 2) this temperature was used to determine $R(T)$, which was approximated by a simple polynomial,
- 3) the polynomial $R(T)$ was then inserted into equation (2) and steps 1 and 2 were iterated until the solutions converged to 5%.

4 DEVICE RESULTS

4.1 Anneal

Prior to performing measurements on the new, high temperature emitter array, we annealed the pixels using the optimal method determined in the materials study. The anneal was performed at maximum power for more than 8 hours, after which the apparent temperature was found to be stable to less than 0.2 K over 100 minutes at 540K. The anneal curve obtained at the emitter level was precisely what was expected based on the materials work performed several months earlier, indicating a stable and repeatable process, validating the knowledge obtained in the materials study and confirming the utility of the constructed models. The anneal curve is shown in Figure 4, from which we note that the total, peak-to-peak change in the apparent temperature over the initial 8 hours was only ~8K and that the temperature variation was less than 1K after the initial 5 hours of annealing.

After the anneal was performed, the stability was then measured at $\frac{3}{4}$ power (the $\frac{3}{4}$ power level was somewhat arbitrary, and we expect to observe similar behavior almost all the way up to the anneal conditions). The stability is shown in Figure 5, from which we see that the apparent temperature is stable to less than 0.2K/hour. This level of stability is consistent with that of the IR camera used to make this measurement, so we take the value of 0.2K/hr as an upper limit to the stability of the new Mirage emitter pixels.

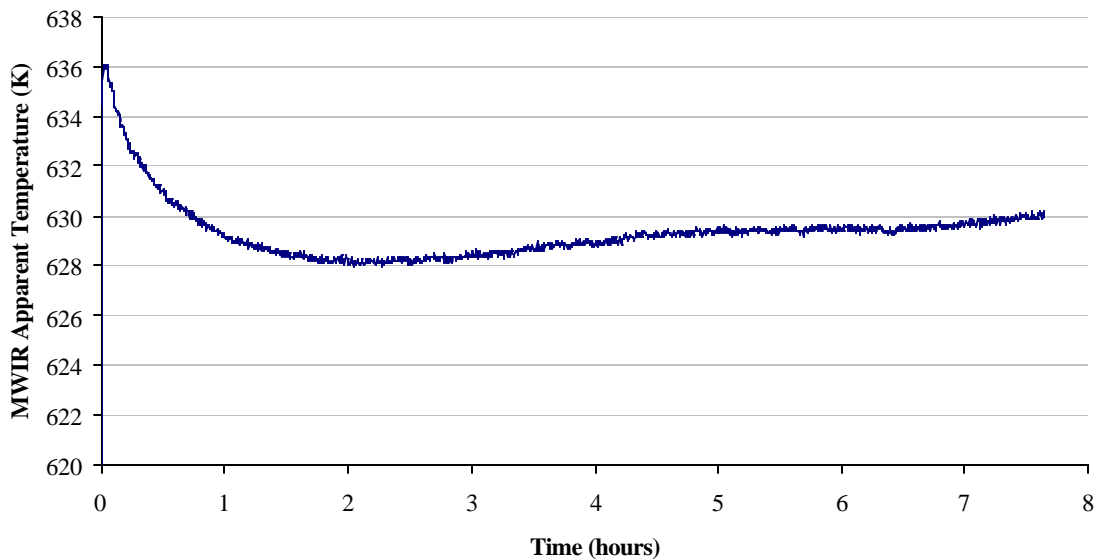


Figure 4 – Anneal data showing the measured MWIR apparent temperature as a function of anneal time. The peak to peak change in the apparent temperature is seen to be ~8K.

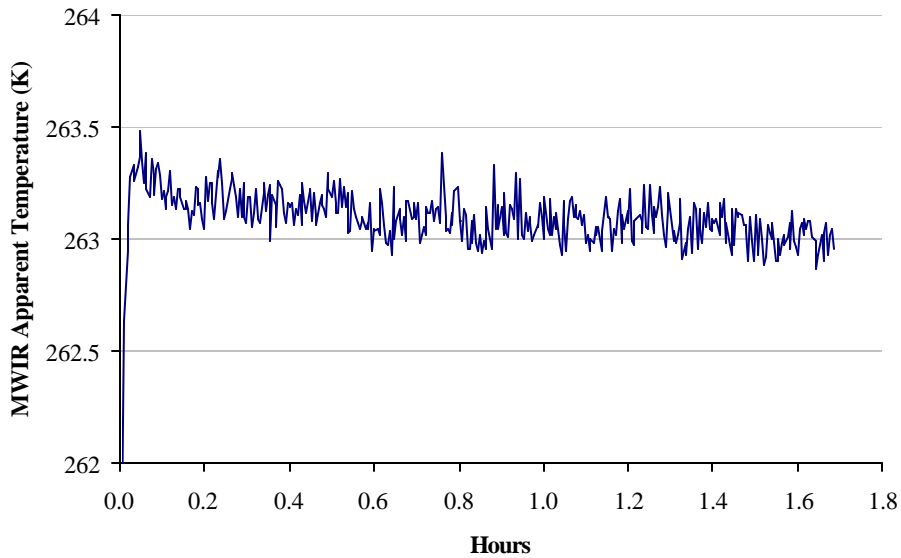


Figure 5 – Post-anneal stability of the new, high temperature Mirage emitter pixels.

4.2 Apparent temperature

MWIR apparent temperatures were measured with an InSb camera and optics that resulted in 1 emitter pixel mapped onto 2×2 camera pixels. The camera was calibrated using an SBIR blackbody over the range 290K–800K, and the camera counts resulting from exposure to the emitter operating at a variety of power levels were compared to the calibration curve to determine the apparent temperature, linearly interpolating where necessary.

We have achieved 700K MWIR apparent temperatures at pixel currents $\sim 66\mu\text{A}$ for mating 14, the mating to which we applied the results of the materials study & model analyses. The CMOS RIIC chip has the built-in capability of adjusting the power applied to the pixels by applying an externally supplied bias. We expect to achieve MWIR apparent temperatures considerably in excess of 700K by use of this capability.

Figure 2 shows the steady state model predictions along with the measured apparent MWIR temperature as a function of pixel current. The emitter resistance as function of temperature was measured and incorporated into the model, and it is seen that the model predicts the MWIR apparent temperature to a high degree of accuracy. Validation of the model is important for future development and improvement.

4.3 Emissivity

The emissivity was measured using a radiometer containing a single element detector with a high spectral resolution CVF ($\Delta\lambda/\lambda \sim 0.02$). This data was then corrected for the detector response and optics transmission (which were measured separately). Dividing the resultant by the radiance curve for a blackbody plus background contributions then yields the spectral emissivity of the emitter pixels. The results of these measurements are presented in Figure 6. These data are consistent with the improvement obtained in the MWIR maximum apparent temperature.

Emissivity models were constructed using the characteristic matrix formalism³ where normal incidence was assumed. These models were used to modify the emitter cavity stack geometry to increase the emissivity. The optical constants were crucial to using this method to predict the emissivity. While the agreement between the model and the measured data is marginal, the average emissivity levels are in rough agreement and the shape of the curves is comparable over the range 2–14 μm . This model is presently under revision to include the effects of the heater fill factor, which is expected to result in better agreement with the measured data.

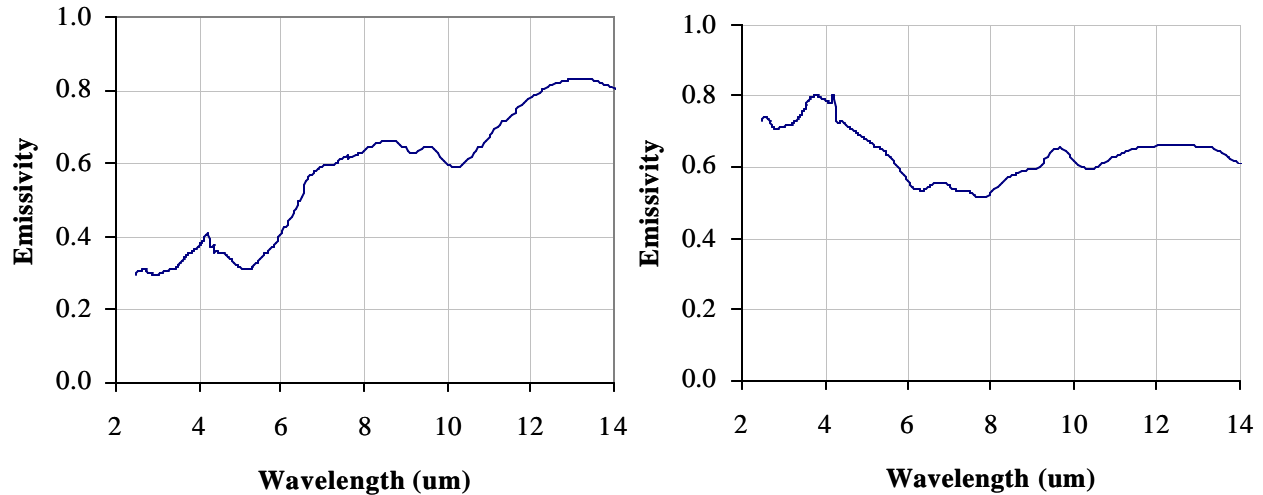


Figure 6 – Emissivity measurements for the baseline emitter (left, M13) and the new, high temperature emitter (right, M14).

4.4 Temporal response

There are two components that contribute to the observed temporal response of the Mirage pixels: 1) the inherent speed of the pixel as given by equation (1) along with the pixel geometry and material properties, and 2) effects due to the RIIC. The latter refers to the two operational modes of the RIIC which show differing temporal behaviors, which are discussed below. The solution to equation (1) shows that the pixel temperature is exponential in time, with a time constant given by m/k , where m is the thermal mass of the pixel (Joule/K) and k is the leg conductance (Watt/K). Infrared detectors measure signal radiance, rather than temperature, and so the temporal response measurements do not show an exponential behavior with time (except for small temperature changes). The Stefan-Boltzmann law dictates that the total power emitted by a blackbody scales with the fourth power of the temperature, while the Wien displacement law shows that the peak radiance from a blackbody is inversely proportional to temperature⁴. Thus the temporal behavior is a strongly non-linear function of temperature, which results in the radiance rising more slowly than the temperature while falling more rapidly than the temperature. These results, expected on theoretical grounds, have been verified by many in the scene generator community, and we have observed the same behavior in the Mirage emitter array.

4.4.1 Snapshot Mode

In snapshot mode, the entire projected frame is updated simultaneously. This is accomplished via switching the signal between a pair of capacitors in each pixel, one storing the next frame’s data while the other drives the emitters with the current frame’s data. When the next frame’s signal is switched from one capacitor to the next, the signal charge is shared between the two capacitors. This results in requiring 2 frames for the signal to reach 90% of its final value *regardless of frame rate*. The overdrive mechanism seeks to overcome this limitation by initially applying more voltage to the pixel than is required by the image being projected in order to drive to the final temperature faster. Conversely, the fall time can be decreased by initially applying less voltage to the pixel than is required by the image. Overdrive mode has been validated, resulting in 5ms rise and fall times at 200Hz frame rates. The method is limited in its operation to the mid 30% of dynamic range simply because the overdrive voltage cannot exceed the dynamic range of the unit cell circuitry, which is ultimately limited by the voltage supply rails of the CMOS process and the signal chain circuitry. The overdrive data has been shown elsewhere in these proceedings².

Figure 7 shows the measured rise time for the new, high temperature emitter. From the figure, it can be seen that the 1/e radiance rise time is 7ms and the 10%–90% rise time is 14ms. Also shown in the figure is the predicted rise time based on the solution to equation (1) along with the factors discussed in section 4.4, which were calculated from established thermal

equilibrium radiation theory⁴. The agreement between the model and the measured response will permit us to reduce the rise and fall times by appropriate changes in materials and geometry in a controlled manner, since we have a physical understanding of the various contributions to the temporal response.

4.4.2 Raster Mode

Raster mode, or rolling-update, updates each pixel sequentially, and the charge sharing between the two capacitors in the unit cell is eliminated because the input voltage is applied directly to each emitter. This mode of operation provides the best measure of the “true” emitter time constant. The present generation of emitters show 12-17ms rise and fall times (10%–90%) with no frame rate dependence.

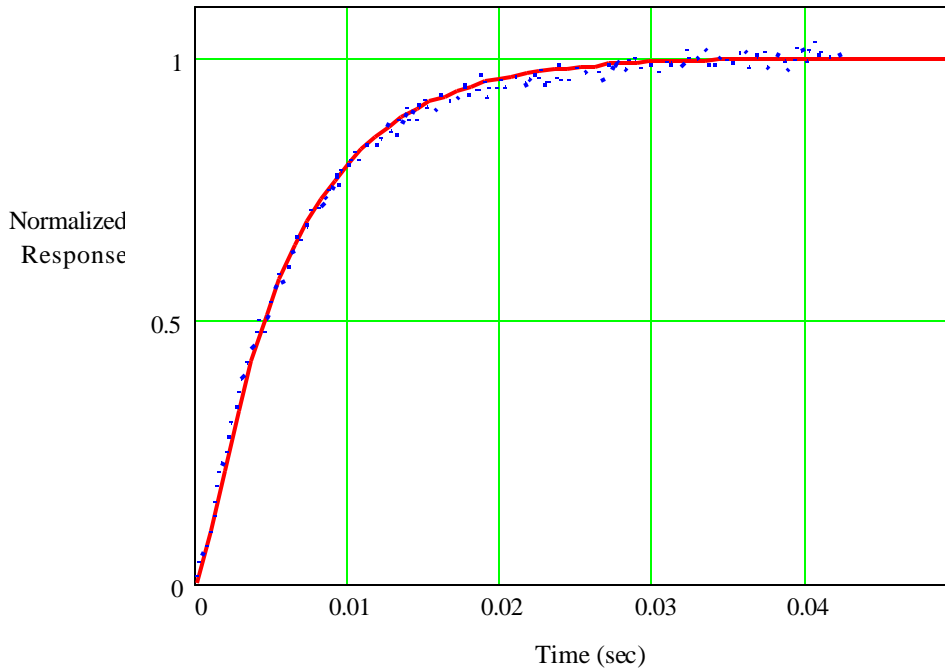


Figure 7 – Radiance rise time measured for mating 14 (dots) along with the model predictions from equation (1).

5 FUTURE PLANS

SBIR is committed to continued improvement in emitter performance and technology. A short list of our plans for the immediate future include:

- ⇒ Continue to push the envelope on maximum apparent temperature
- ⇒ Further improvement of anneal process
- ⇒ Achieve 5ms rise time (10-90%) via geometry and materials optimization
- ⇒ Develop a family of emitter arrays to meet specific application requirements
 - Cryogenic operation
 - High speed
 - High temperature
- ⇒ New pixel designs for 1024x1024 array

6 SUMMARY

The Mirage emitter array has attained MWIR apparent temperatures of 700K as the result of an extensive materials characterization study. A robust anneal process has been developed which results in very stable apparent temperatures ($<0.2\text{K}$ over 1 hour). Physics-based models have been constructed and validated by extensive device measurements, and will serve to provide the framework within which future improvements will be made. The emitter fabrication process has been improved through the use of advanced diagnostic techniques, resulting in high yield and excellent operability.

7 REFERENCES

- [1] S. McHugh, J. Warner, M. Pollack, A. Irwin, T. Hoelter, B. Parrish, and J. Woolaway, "MIRAGE Dynamic IR Scene Projector Overview and Status", SPIE Proceedings Vol. 3697, Orlando, Florida, pp. 209-222, 1999.
- [2] J. Oleson, K. Sparkman, A. Irwin, L. Rubin, S. McHugh, S. Solomon, "MIRAGE: System Overview and Status," SPIE Proceedings, Vol. 4366, Orlando, Florida, 2001.
- [3] M. Born, E. Wolf, "Principles of Optics," Cambridge University Press, Cambridge, UK, 1999.
- [4] G.H. Wannier, "Statistical Physics," Dover Publications, New York, 1966.

CORRESPONDENCE

For more information please contact:
Jim Oleson
Santa Barbara Infrared, Inc.
Telephone: 805-965-3669
Fax: 805-963-3858
e-mail: joleson@sbir.com